JOURNAL OF CATALYSIS **168,** 450–462 (1997)
ARTICLE NO. CA971637

Tantalum-Pillared Montmorillonite

I. Synthesis and Physicochemical Characterization

G. Guiu, A. Gil, M. Montes,* and P. Grange

*Catalyse et Chimie des Matériaux Divisés, Université catholique de Louvain, Place Croix du Sud 2/17, 1348 Louvain-la-Neuve, Belgium; and *Grupo de Ingenieria Quimica, Universidad del Pais Vasco, San Sebastian, Spain*

Received October 17, 1996; revised January 15, 1997; accepted January 15, 1997

The synthesis method of a stable, large-pore tantalum-pillared montmorillonite family (Ta-PILC) and its physicochemical characterization are reported. The clay used is a sodium montmorillonite. The tantalum pillaring solution is prepared by careful control of the hydrolysis of a tantalum alkoxide precursor, $Ta(OC_2H_5)_5$, in an ethanolic acidic solution. From XRD analysis it has been concluded that the Ta-PILC possesses a high thermal stability, the pillared structure is preserved even after calcination at 600°C, and the basal spacing, 26 Å at 500°C, is one of the greatest values described in the literature. On the basis of the bibliographic data concerning tantalum alkoxide hydrolysis and condensation, and taking into account the experimental results obtained for this series of Ta-PILCs, a structure of type $[Ta_8O_{10}(OR)_{20}]$, $R = H, C_2H_5$, has been proposed as the precursor molecule of the tantalum pillars.

INTRODUCTION

Pillared clays (PILC) are microporous solid acid materials prepared by intercalating a metal oxide precursor between the layers of an expandable clay mineral. After calcination, a bidimensional zeolite-like structure is obtained. The size of the micropores is generally larger than those in the conventional zeolite cage. The dimension of the microporous structure as well as the acid-base properties of the PILC depend on the nature of the chosen pillar precursor and on the pillaring conditions. Many PILCs have been prepared using polycationic species of Ti, Cr, Fe, Ni, Zr, Al, Ga, and Si. Of these, the materials using Al(III) and Zr(IV) species appear to have the most promising properties: stable up to 500°C and surface areas up to 200 m^2/g. Several reviews on PILCs have already been published (1, 2).

The diversity of the precursors studied is proof of the great interest of pillared clays in catalysis. Therefore, the enlargement of the PILC family with new pillar precursors promises to be an interesting advancement in this field.

The acid-base properties of tantalum oxide have been studied recently and much interest has been shown in Ta_2O_5, particularly in its hydrated form, also known as tantalic acid, which shows high acidity strength: Hammet acidity function (3) $H_0 = -8.2$ (90% H_2SO_4). Tantalum oxide can be considered a solid with unusual acid properties. Whereas most of the metal oxides show acidity after calcination at 500°C, tantalum oxide shows maximum acidity at relatively low temperatures: 100–300°C. On the other hand, whereas the acidity of the metal oxides decreases after water absorption, the acidity of tantalum oxide is maintained even after absorption of large amounts of water. Therefore, this solid acid is favorable to the development of stable catalytic activity in reactions where water molecules are present. Indeed, it shows excellent stability in esterification, hydration, and dehydration reactions (4–6).

As a result of the factors described above, the intercalation of such solid acids between the layers of an expandable clay would produce catalysts with acid properties different from those of conventional pillared clays.

Nevertheless, in the case of tantalum as the precursor of the pillars, the formation of metallic polyhydroxides in water, which is the easiest way to the PILC synthesis, is limited by the complicated chemistry of the tantalum ion in aqueous solution (7, 8).

This probably explains why only one attempt of clay intercalation with tantalum has been reported in the literature. Christiano *et al.* (9) have chosen an alternative way of using metallic polyhydroxides. Indeed, these authors have used a tantalum cluster $[Ta_6Cl_{12}^{2+}]$ (10) as the precursor of the pillars, which, after intercalation, is hydrolyzed and oxidized *in situ*. After calcination at 350°C, the solid obtained exhibits a surface area of 70 $m^2\ g^{-1}$ and a basal spacing of 19.1 Å. This pillared clay collapses at 400°C.

The aim of this paper is to describe the synthesis method of a stable, large-pore tantalum-pillared montmorillonite family (Ta-PILC) and to report the results of its physicochemical characterization. The preliminary results of this study have already been published as a short communication (11).

0021-9517/97 $25.00

METHODS

Catalyst Preparation

The experimental conditions for the elaboration of the precursor solution of the pillars were set up through a careful study of the influence of: (i) the choice of the tantalum initial species ($TaCl_5$, TaF_5, and $Ta(OC_2H_5)_5$ were studied) and (ii) the nature of the solvent (water or alcohol). The tantalum alkoxide precursor and anhydrous ethanol solvent appeared to be the most suitable choices. Once the general procedure for the synthesis of Ta-PILC was fixed, we studied the influence of one of the main preparation parameters, the Ta/clay ratio (mmol Ta/g of clay), on the thermal stability, texture and acidity. Indeed, the content of tantalum versus the quantity of clay is one of the main experimental parameters to study for the optimization of the synthesis method (12).

The clay used was a commercial sodium montmorillonite, Kunimine-Pure F, obtained from Kunimine Industry Co. Ltd, with a particle size of less than 2 μm and a cationic exchange capacity (CEC) of 106 meq/100 g of clay. Before pillaring, this sodium montmorillonite was dispersed in water and aged for 1 month. It was then washed by dialysis until the conductivity of the surrounding water was less than 1.5 μS. Eventually, the solid content of the clay suspension was adjusted to 10 g clay liter^{-1}. Fifty milliliters of Na-montmorillonite dispersion was used for each synthesis. Before the intercalation process, a 10% (v/v) acetic acid solution (96%) was added to the clay suspension.

The tantalum pillaring solution was prepared by careful control of the hydrolysis of a tantalum alkoxide precursor (Aldrich, $Ta(OC_2H_5)_5$, 99.98%). The quantity of tantalum ethoxide required, imposed by the chosen Ta/clay ratio, was dissolved in 200 ml of anhydrous ethanol (Carlo Erba, 99.5%). The hydrolysis ratio was then adjusted to $H_2O/Ta = 5$ and the solution stirred for 20 min at room temperature. The initial concentration of the tantalum alkoxide in the clay suspension was varied between 0.77 and 6.17 mmol Ta/g of clay. Details of initial tantalum content for all catalysts are given in Table 1.

In the pillaring process, the Na-montmorillonite suspension was added dropwise (addition rate 7 ml/min), with continuous stirring, to the precursor solution of the tantalum pillar. The final suspension was allowed to stand for 3 h, with vigorous stirring at room temperature. The suspension was then washed by centrifugation (7×10^3 rpm) to constant conductivity. Eventually, the samples were then dried overnight and calcined in subsequent successive steps: 120, 250, and 500°C.

Physicochemical Characterization

The XRD spectra were recorded in the 2θ range of 1.5° to 20°, sweeping rate 0.2°/min, with a Kristalloflex Siemens D5000 diffractometer using Cu $K\alpha 1$ radiation and a secondary monochromator. A Ni filter was used. The results obtained were processed using a Diffrac-AT V3.0 measurement system. In preparation for XRD analysis, a few drops of sample suspension were deposited on glass slides and dried at room temperature. Since pillared clays usually show a broad XRD pattern, the use of oriented specimens is helpful for measuring the basal spacing unambiguously. The interlayer distance of pillared clays was obtained from its first-order reflection, $d(001)$. The evolution with the thermal treatment, carried out *in situ*, was studied over a temperature range between 100 and 600°C. A spectrum was recorded at an interval of every 100°C, after 1 h at constant temperature.

The XRD spectra of Ta-PILC calcined at 700 and 900°C were also recorded for 2θ between 2° and 70°, with a sweeping rate of 0.5°/min. The samples, in powder form, were analyzed after deposition on a quartz monocrystal sample holder supplied by Siemens.

The differential thermal analysis (DTA) and the thermogravimetric analysis (TGA) were performed using a Setaram TGA 92 apparatus with a heating rate of 10°C/min, over a temperature range of 120–1000°C. The quantity of sample used for these analyses was about 30 mg. Before analysis the samples were dried at 120°C for 2 h, thus allowing elimination of water and alcohol adsorbed on the external surface and in the microporous volumes created by pillaring.

Transmission electron microscopy (TEM) of samples was carried out using a Jeol TEM SCAN 100 CX instrument, coupled with a Kevex 5100 energy dispersion spectrometer. The electron acceleration tension was 100 kV.

The silicon, aluminum, tantalum, and sodium contents in Ta-PILC were estimated by atomic absorption spectrophotometry.

Nitrogen adsorption experiments were performed at 77 K in a Micromeritics ASAP 2000 apparatus using a static volumetric method. The samples calcined at 500°C were previously degassed at 100°C for 4 h to a final pressure of 1 mm

TABLE 1

Sample Nomenclature and Initial Tantalum Content (mmol Ta/g of Clay) for This Series of Ta-PILC

Samples	Ta/clay ratio [mmol/g]
PILC-[Ta]1	0.77
PILC-[Ta]2	1.54
PILC-[Ta]3	2.31
PILC-[Ta]4	3.08
PILC-[Ta]5	3.86
PILC-[Ta]6	4.63
PILC-[Ta]7	5.40
PILC-[Ta]8	6.17

Hg. The specific total surface areas were obtained for the range of 0.05 to 0.2 of partial pressures using the BET equation and the microporous volumes were calculated using the α_S-plot method (13, 14). Total pore volumes were estimated from nitrogen uptake at $P/P_0 = 0.99$.

An exhaustive micropore characterization, in order to obtain the micropore size distribution of the sample, was achieved through the adsorption isotherms starting at much lower relative pressures (10^{-6}) than those used in conventional analysis.

Infrared (FTIR) spectra were recorded using a Brucker FT 88 spectrometer. The samples were diluted in KBr at a concentration of 10% wt Ta-PILC, and pressed in pellets. In preparation for FTIR analysis, the pellets were dried in vacuum (10^{-6} Torr) at 150°C for 2 h. The spectra were recorded directly at room temperature.

The photoelectron spectroscopy (XPS) studies were performed at room temperature on SSX-100 "206 Surface Science Instruments (SSI)" equipment (10 kV, 11.5 mA). The X-ray source was an Al anode (1486.6 eV), supplied by a monochromator. The energy scale of the spectrometer was calibrated with the Au $4f_{7/2}$ binding energy fixed at 83.98 eV. The atomic concentration ratios were calculated by correcting the intensities (the integral of each peak) with the sensitivity factors (15).

In preparation for the analysis, the samples were degassed under vacuum (10^{-7} Torr) for at least 10 h at room temperature. The residual pressure in the spectrometer during the analysis was between 5 and 10×10^{-9} Torr. The positive charge generated by the photoelectron ejection process within the insulating samples was made up by using a charge neutralizer. The neutralizer energy was adjusted at 8 eV.

RESULTS

X-Ray Diffraction

XRD patterns of Ta-PILCs calcined at several temperatures (100–600°C) recorded in the range of 2θ from 2° to 12° are shown in Fig. 1. The Ta-PILC diffractograms show two first-order reflections (d(001)). The first at $2\theta \approx 7°$ can be assigned to the nonpillared clay during the intercalation process. The second at $2\theta \approx 3°$, because the intercalation of tantalum polyhydroxides between the montmorillonite sheets results in an increment of the basal spacing, corresponds to the pillared clay. For the highest tantalum contents, i.e., PILC-[Ta]7, the 7° reflection is broader and contains two maxima. The maximum at 2θ, slightly lower, could be the result of the intercalation of tantalum species different from those giving the pillared structure.

As can be observed from Fig. 1, when the tantalum content used in the intercalation process increases, an increase in the intensity of the pillared clay d(001) peak and a decrease in the intensity of the nonpillared d(001) peak are

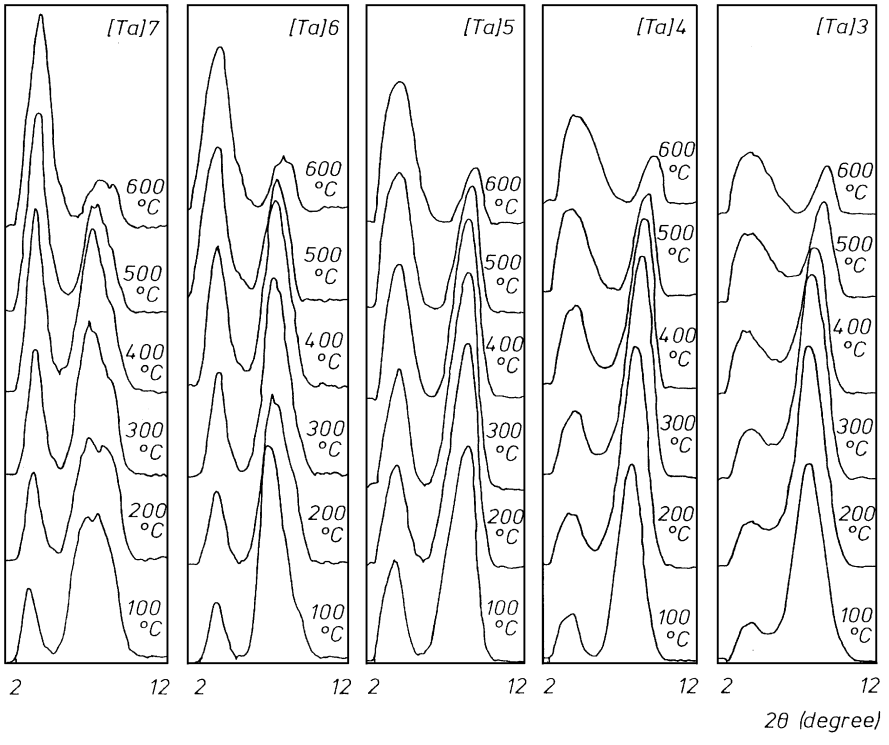

FIG. 1. Evolution of XRD patterns of Ta-PILCs as a function of calcination temperature.

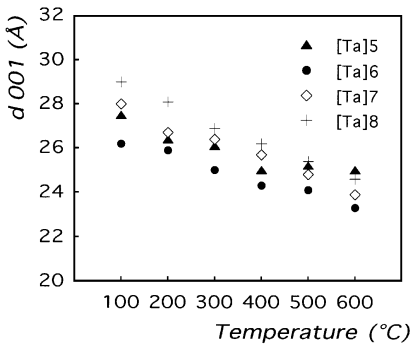

FIG. 2. Evolution of basal spacing (Å) of pillared clays with thermal treatment.

noted, for the same thermal treatment. In addition, as can be seen in Fig. 1, a minimal quantity of mmoles of Ta per gram of clay (≈3.86) seems to be required in order to obtain a solid characterized by a well-defined pillared clay diffraction peak.

The thermal stability of these products was studied by comparing the evolution of the Ta-PILC interlayer distances at different temperatures (Fig. 2). The interlayer distances measured for all the products of this series of Ta-PILCs are considerable. Although the basal spacing for all samples decreases with increase of the calcination temperature, the values obtained for products calcined at 500°C (24–26 Å) show that the pillared structure is maintained even after this thermal treatment. We reported only the values corresponding to the PILC-[Ta]5, PILC-[Ta]6, PILC-[Ta]7, and PILC-[Ta]8 samples, since for the solids with low tantalum content the resolution of the X ray diffraction is not good enough to evaluate the basal spacing precisely whatever the calcination temperature.

XRD patterns of PILC-[Ta]3 and PILC-[Ta]7 samples calcined at 700 and 900°C recorded with 2θ from 2° to 70° are displayed in Figs. 3A and 3B, respectively.

The crystallization of pure tantalum oxide into the orthorhombic phase occurs at 760°C (16). However, as can be seen in Figs. 3A and 3B, after thermal treatment at 900°C PILC-[Ta]3 and PILC-[Ta]7 present only slight peaks corresponding to the more intense lines of the tantalum oxide orthorhombic phase. At 700°C, the temperature at which the dehydroxylation of the montmorillonite sheets occurs, the Ta-PILC loses its pillared structure. This dehydroxylation, and the fact that the spectrum of PILC-[Ta]7 calcined at 700°C has been taken with a sample in powder form, explains the dramatic loss of the 3° diffraction peak in Fig. 3B compared to Fig. 1.

Thermal Analysis

In the range of 120 to 700°C, thermogravimetric analysis of tantalum-pillared clays shows a constant decrease in sample weight with increasing temperature. The weight loss varies between 4 and 5% of the weight of the sample dried at 120°C.

Figure 4 shows TGA curves as well as their differential form (DTG) for the sodium montmorillonite and Ta-PILCs.

For the Ta-PILCs, several temperature ranges can be distinguished. The TGA and DTG analyses strongly suggest that the dehydroxylation of the pillars is carried out between 200 and 400°C. In fact, these curves present two maxima in this range. The first, at about 190°C, can be assigned to the elimination of hydration water, which could be more strongly bonded than in nonpillared clays, probably either by hydrogen bond or coordinated to the pillars (17, 18). The second, at about 330°C, can be associated to the dehydroxylation of the pillars. Between 600 and 620°C, there is an extra weight loss assigned to the elimination of water produced by dehydroxylation of the clay sheets. Its intensity per gram of sample decreases with an increase in tantalum content.

For sodium montmorillonite, the most remarkable desorption is observed at about 686°C. That is, the dehydroxylation of the clay sheets in Ta-PILC is done at a temperature about 68°C lower than that in sodium montmorillonite.

The differential thermal analysis of sodium montmorillonite shows an endothermic peak due to the dehydroxylation of the clay structure at 690°C. Besides, an exothermic transition, assigned to the formation of spinelle, albite, quartz, and enstantite, is also observed at 950°C (19).

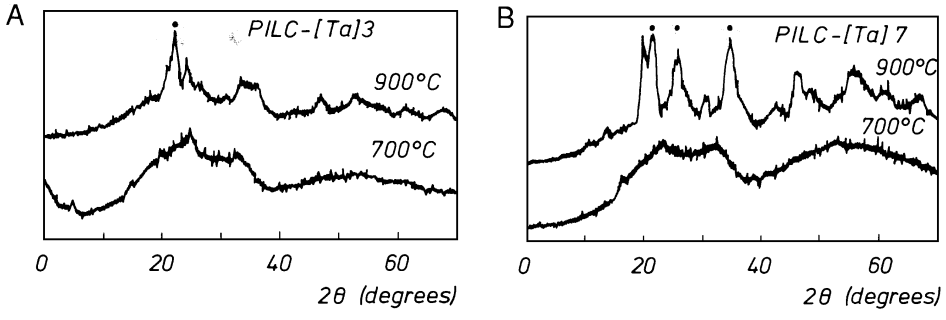

FIG. 3. (A) XRD patterns of PILC-[Ta]3, 2θ 2°–70°, after thermal treatment at 700 and 900°C. (B) XRD patterns of PILC-[Ta]7, 2θ 2°–70°, after thermal treatment at 700 and 900°C.

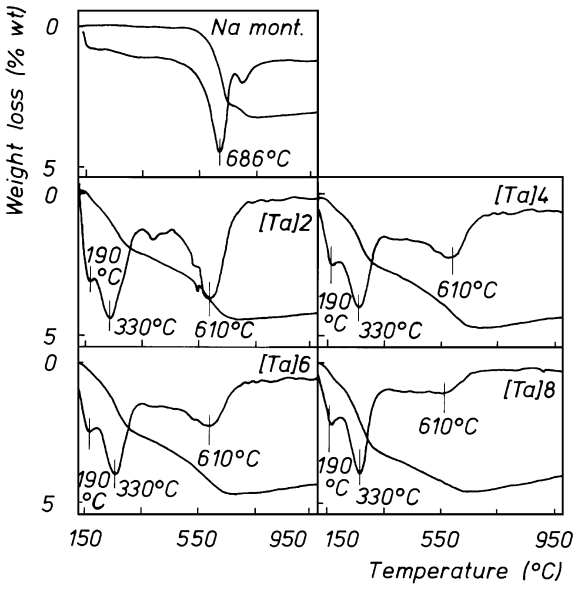

FIG. 4. TGA and DTG curves for Ta-PILCs and Na-montmorillonite.

The DTA analysis of tantalum-pillared clays presents the peak assigned to the dehydroxylation of the clay structure at lower temperatures (630°C) than Na-montmorillonite. The Ta-PILCs show, in addition to two peaks of Na-montmorillonite, the existence of another exothermic transition at 870°C. This transition, detected from tantalum contents higher than 3.08 mmol Ta/g of clay, can be associated with the tantalum pillars. However, it would correspond to the amorphous tantalum oxide crystallization. The intensity of this exothermic peak increases with the tantalum content of Ta-PILC. Under the same experimental conditions, amorphous pure tantalum oxide crystallizes at 760°C. Therefore, in Ta-PILCs, the tantalum oxide crystallization process is delayed by about 100°C.

Atomic Absorption Spectrometry

The results of atomic absorption spectrometry analysis, expressed as percentage weight of oxide, are summarized in Table 2. Figure 5 shows the value, in mmol Ta/g of clay, of the final tantalum content obtained by atomic absorption analysis of the Ta-PILCs versus the initial tantalum content in the intercalation process.

The final tantalum content (mmol Ta/g of clay) was calculated taking into account (i) the percentage weight of Ta_2O_5 and SiO_2 in Ta-PILC (Table 2) and (ii) the percentage weight of the SiO_2 within the montmorillonite layer (58%).

Initially, the tantalum concentration in pillared clays increases linearly with the increase of the quantity of tantalum used in the intercalation process. However, from the sample PILC-[Ta]5, the curve seems to reach a plateau. Since the maximum quantity of tantalum used for the intercalation is much greater than the final tantalum content in Ta-PILCs, the excess of tantalum must be eliminated during the settling and subsequent successive washings of the final product. This was confirmed by the analysis of the washing water which shows a very high content of tantalum for the PILC-[Ta]5, PILC-[Ta]6, PILC-[Ta]7, and PILC-[Ta]8 samples.

TABLE 2

Ta-PILC Chemical Analysis Expressed as Percentage Weight of Oxide

Samples	% Oxide			
	SiO_2	Al_2O_3	Ta_2O_5	Na_2O
Na-mont.	60.9	21.4	0.0	2.70
PILC-[Ta]2	48.9	16.6	24.5	0.10
PILC-[Ta]3	39.8	13.5	34.7	0.08
PILC-[Ta]4	36.0	12.1	42.1	0.08
PILC-[Ta]5	33.4	10.6	43.5	<0.07
PILC-[Ta]6	31.5	10.3	48.3	0.07
PILC-[Ta]7	29.3	9.5	51.1	0.09
PILC-[Ta]8	29.6	9.2	53.2	0.10

The SiO_2/Al_2O_3 ratio in pillared clays varies between 2.9 and 3.1. Taking into account the 2.9 ratio obtained for the initial Na-montmorillonite and the experimental error (up to 3% for each element), the ratios obtained for the Ta-PILCs seem to show that the structure of the clay sheets was not impaired during the intercalation process.

The Na_2O content in Ta-PILCs dried at 120°C varies between 0.07 and 0.10% in weight. Compared with the 2.7% in the initial Na-montmorillonite, these results indicate that the cationic exchange of sodium in the intercalation process, by species derived from tantalum, is almost complete for the entirety of analyzed samples.

Textural Characteristics

The nitrogen adsorption–desorption isotherm for Na-montmorillonite and an isotherm representative of the

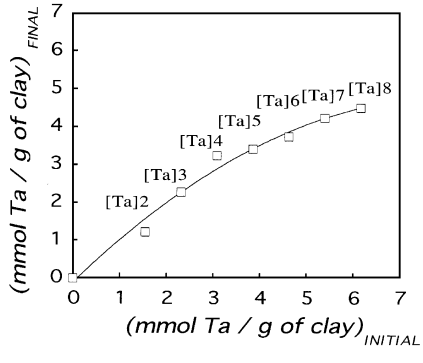

FIG. 5. Values, in mmol Ta/g of clay, obtained by atomic absorption analysis of the Ta-PILCs versus the initial tantalum content in the intercalation process.

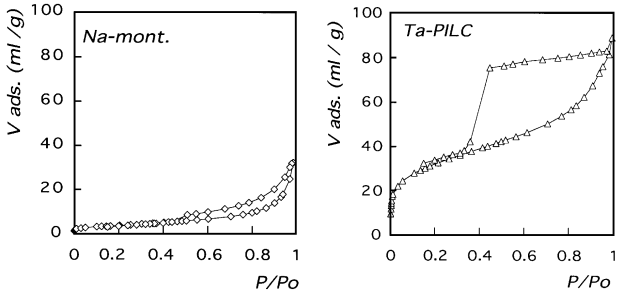

FIG. 6. Nitrogen adsorption–desorption isotherm for Na-montmorillonite and an isotherm representative of the shape found for the Ta-PILCs (PILC-[Ta]6).

shape found for the Ta-PILCs (sample PILC-[Ta]6) are displayed in Fig. 6. The samples analyzed were previously calcined at 500°C.

The adsorption isotherm for Na-montmorillonite calcined at 500°C is type II according to the Brunauer, Deming, Deming, and Teller (BDDT) classification (macroporous solids). The hysteresis loop (H3 type in IUPAC) indicates the presence of slit or parallel plates shaped mesoporous.

The Ta-PILC adsorption isotherms are of a mixed type corresponding to a combination of type I and II isotherms. In fact, at low relative pressures, the isotherms show a high uptake of nitrogen, characteristic of type I isotherms, indicating therefore the presence of micropores within the Ta-PILCs. Otherwise, at high relative pressures ($P/P_0 > 0.4$) the adsorption isotherm can be associated with a type II isotherm, characteristic of macroporous solids. The hysteresis loop is type H3 in the IUPAC classification. Namely, the adsorption–desorption isotherms show that this series of Ta-PILC possesses, in addition to the characteristic microporosity of PILCs, a mesomacroporous structure.

The BET surface areas and the pore volumes of the tantalum-pillared clays are given in Table 3. The micropore

TABLE 3

Specific Surface Areas and Specific Pore Volumes for Ta-PILC

Samples	S_{BET}[a]	C[b]	$S_{ext.}$	V_p[c]	$V_{\mu p}$[d]
Na-mont.	14	100	14	0.050	0.000
Ta_2O_5	56	215	56	0.04	0.0
PILC-[Ta]1	139	296	89	0.165	0.027
PILC-[Ta]2	116	239	73	0.134	0.026
PILC-[Ta]3	114	209	59	0.138	0.027
PILC-[Ta]4	125	230	65	0.161	0.030
PILC-[Ta]5	118	207	52	0.157	0.031
PILC-[Ta]6	125	237	52	0.141	0.040
PILC-[Ta]7	129	227	52	0.149	0.045
PILC-[Ta]8	135	225	43	0.150	0.050

[a] Specific surface area (m^2/g).
[b] BET C value, characteristic of the adsorbate–adsorbent interaction.
[c] Specific total pore volume at P/P_0.
[d] Specific pore volume (cm^3/g).

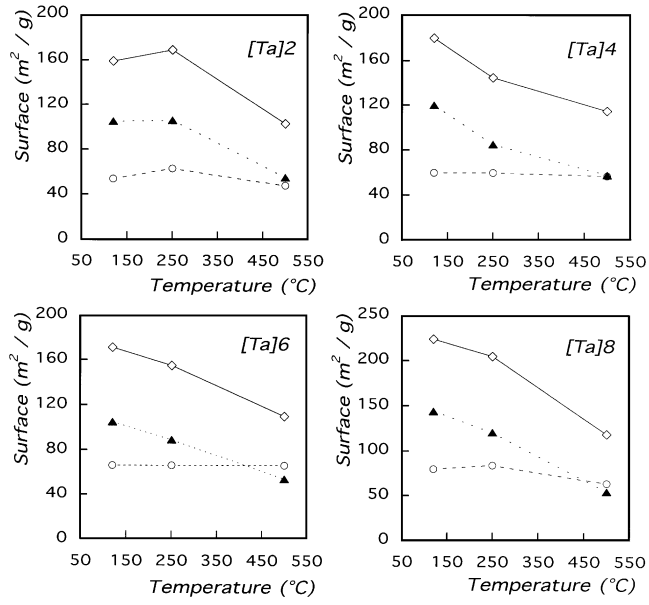

FIG. 7. Evolution of the BET specific surface areas (◇), the external surface areas (○), and the micropore surface areas (▲) as a function of calcination temperature.

volumes and the external surface area were obtained from the α_s-plot method. This method is based on the comparison of the shape of the adsorption isotherm of the sample studied with that of an isotherm of a nonporous reference solid. In this work, a sample of Na-montmorillonite calcined at 800°C was used as a reference solid. The micropore surface areas were calculated by subtracting the external surface area from the total BET area.

Figure 7 shows the evolution of the BET specific surface areas, the external surface areas, and the micropore surface areas of Ta-PILCs versus the calcination temperature.

All the Ta-PILCs, except PILC-[Ta]2, present a continuous decrease in the specific surface area with the calcination temperature. For PILC-[Ta]2, an increase in BET surface area after 250°C calcination can be observed. The thermal treatment seems to have a stronger influence upon the micropore than upon the external surface area.

The nitrogen adsorption isotherm of the tantalum-pillared clays, calcined at 500°C, shows that these solids present a microporous structure. In order to study this microporosity, nitrogen adsorption isotherms were built more accurately at very low pressures. Figure 8 shows the micropore size distribution for tantalum-pillared clays obtained using the slit-like model of Horvath and Kawazoe (20). As recently proposed by Gil and Montes (21), the value of $N_a A_a + N_A A_A$ (named the "interaction parameter") used in this study has been 33.8 cal · nm^4 mol^{-1}.

PILC-[Ta]2, PILC-[Ta]4, and PILC-[Ta]6 microporous distribution curves show two differentiated maxima at 4.2 and 6.3–6.6 Å. For these samples, a shoulder at about 5.3 Å

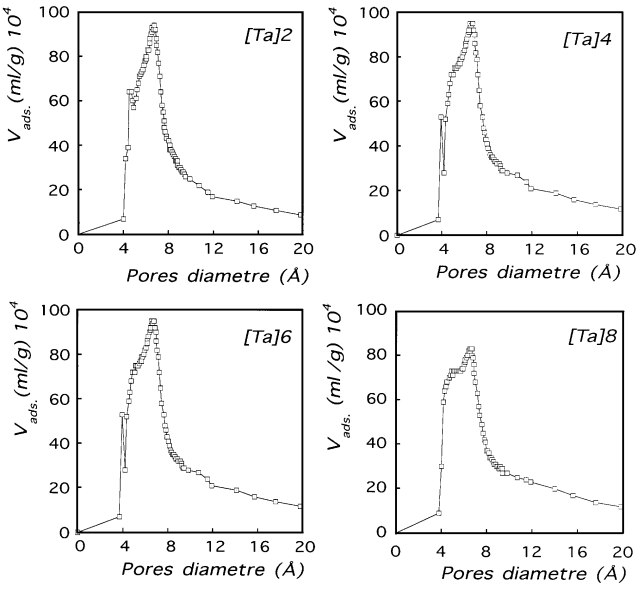

FIG. 8. Micropore size distribution of PILC-[Ta]2, PILC-[Ta]4, PILC-[Ta]6, and PILC-[Ta]8.

can also be observed. However, a bimodal micropore distribution was obtained for PILC-[Ta]8. Indeed the maximum at 4.2 Å disappears and the 5.3 Å shoulder is better differentiated.

Infrared Studies

The FTIR spectra analyses have been divided into two ranges: 2500–4000 and 400–1300 cm^{-1}.

The FTIR spectra in the interval between 2500 and 4000 cm^{-1} are shown in Fig. 9. Two bands are observed in this region. The first, a very sharp symmetrical absorption band, corresponds to Al^{3+}- or Mg^{2+}-bonded OH structural groups. This vibrational mode is detected at 3635 cm^{-1} for Na-montmorillonite (22–24). For Ta-PILCs, the wavenumber at which the maximum of this band appears shifts from 3635 to 3660 cm^{-1}. The maximum position of this band as well as its intensity remains constant for all Ta-PILCs analyzed.

The second band, at lower absorption frequencies (between 3400 and 3600 cm^{-1}), is much larger and nonsymmetrical. The intensity of this band increases with the initial tantalum content in the samples analyzed. Because of the preparation method of these pellets (dried under vacuum at 150°C) and the absence of the water deformation mode at 1635 cm^{-1}, this second band cannot correspond to H-bonded water molecules on the surface. Therefore, this band can be assigned to the vibrational modes of the OH-group on the amorphous tantalum oxide surface.

In the region between 2800 and 3000 cm^{-1} the Ta-PILCs exhibit an absorption triplet (2962, 2915, and 2862 cm^{-1}) which can be associated with the stretching mode of the CH bonds in the ethoxy ligands (25).

The FTIR spectra of this series of Ta-PILCs in the region between 400 and 1300 cm^{-1} are displayed in Fig. 10. In the range 800 to 1200 cm^{-1}, the spectra of Ta-PILCs are very similar to that of Na-montmorillonite. The Si–O and Si–O–Si stretching modes and the Al^{3+}- and Mg^{2+}-bonded OH group deformation modes are observed in this range. The M–OH and Si–O deformation modes as well as the Si–O–Al stretching mode appear in the region between 400 and 800 cm^{-1}. The vibrational modes observed in this region for PILC-[Ta]1 and PILC-[Ta]3 correspond to those of pure Na-montmorillonite. The Ta-PILCs with a tantalum content higher than that of PILC-[Ta]3 show, in addition to the characteristic vibrational modes of Na-montmorillonite, a large band at 654 cm^{-1} which can be associated with the Ta–O bond stretching mode (26, 27). This band is hardly visible for PILC-[Ta]5 but its intensity increases with the tantalum content of the samples (PILC-[Ta]6 < PILC-[Ta]8).

In the region 400 to 800 cm^{-1}, the FTIR spectra of Ta-PILCs show a great decrease in the intensity of Si–O–Al stretching and Si–O deformation modes with the tantalum content. This phenomenon can be related to the decrease in clay content per gram of PILC when the tantalum content increases.

X-Ray Photoelectron Spectroscopy

XPS is a technique for analyzing the outermost layers of the solids (about 30 Å on average). XPS allows one to obtain

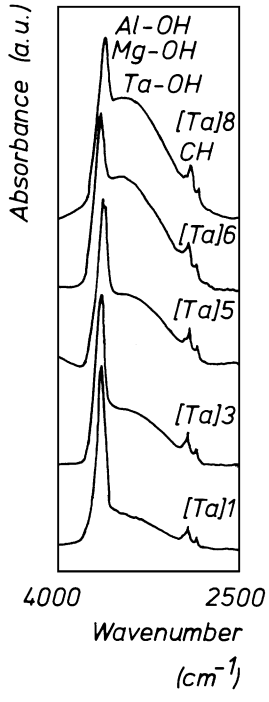

FIG. 9. FTIR spectra in the interval between 2500 and 4000 cm^{-1} for PILC-[Ta]1, PILC-[Ta]3, PILC-[Ta]5, PILC-[Ta]6, and PILC-[Ta]8.

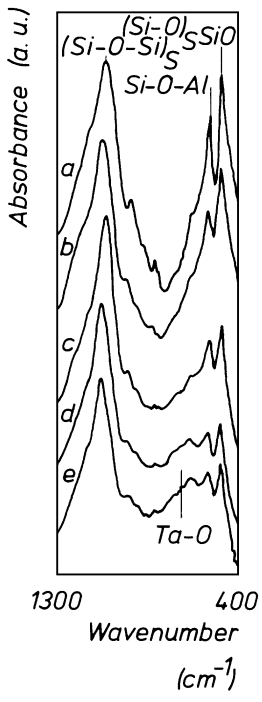

FIG. 10. FTIR spectra in the interval between 400 and 1300 cm^{-1}. (a) PILC-[Ta]1, (b) PILC-[Ta]3, (c) PILC-[Ta]5, (d) PILC-[Ta]6, and (e) PILC-[Ta]8.

information on the chemical environment of the different elements within the clay crystalline network (28). However, as a result of the montmorillonite structure, which consist of 9.6-Å-thick sheets, for the Ta-PILC this technique will also provide information concerning the pillars in the interlayer space.

The O 1*s*, Si 2*p*, Al 2*p*, and Ta $4d_{5/2}$ core electron binding energies (eV) for Ta-PILCs and for Na-montmorillonite are summarized in Table 4.

In the literature, the method most widely used to make the binding energy scale correction is by fixing the binding energy of the miscellaneous carbon of the samples (C 1*s* peak) at 284.8 eV. When this method was used for the Ta-PILCs the characteristic energies for the totality of the components of the montmorillonite, as well as for the tantalum oxide, shifted to higher binding energies.

This shift to higher binding energies for all the elements can hardly be explained in any other way than by an erroneous energy reference. The importance of the reference chosen for the charge correction has already been studied by Remy *et al.* (29), who noted that the use of the miscellaneous carbon as reference for analyzing the mordenite led to abnormally high binding energies for all the elements. This phenomenon was assigned to the charge difference existing between the zeolite network, where an electric field is developed, and the miscellaneous carbon.

From then on, the scale taking as reference the miscellaneous carbon C 1*s* line at 284.8 eV leads to erroneous binding energies. To solve this problem, an internal standard is required. The Si 2*s* line fixed at 153.4 eV has already been used as reference for the Na-montmorillonite provided by Kuminine Industrial Co. (30). However, in this work, the Mg Auger line has been chosen as reference. Indeed, the magnesium in the montmorillonite octahedral layers will not be as disturbed by the pillars as the silicon in the tetrahedral layers.

In agreement with the values found in the literature, the binding energy taken for the main Mg Auger $KL_{23}L_{23}$ line was 306.0 eV.

Any meaningful variation cannot be observed between the Al 2*p* and the Si 2*p* line binding energies in Na-montmorillonite or in Ta-PILC. In addition, the tantalum Ta $4d_{5/3}$ line in Ta-PILCs appears at exactly the same position as in pure tantalum oxide (31). The tantalum oxide was analyzed taking the C 1*s* line of the miscellaneous carbon at 284.8 eV as reference.

In Ta-PILC, the O 1*s* band is asymmetric, and can be deconvoluted into two components. The position of the main component corresponds to that of the oxygen in Na-montmorillonite. The second oxygen component appears with the intercalation of tantalum polyhydroxides and its intensity increases with the tantalum content. The position of this second oxygen component corresponds to the oxygen in Ta–O–Ta type bond.

TABLE 4

Core Electron Binding Energies (eV) for Ta-PILCs and Sodium-Montmorillonite

Samples	Si 2*p*	Al 2*p*	O 1*s*	Ta $4d_{5/2}$	Ta_2O_5/SiO_2	Al_2O_3/SiO_2
Na-mont.	102.7	74.7	531.9			0.35
Ta_2O_5			532.3	230.2		
			530.8			
PILC-[Ta]4	102.5	74.5	531.7	230.2	0.47	0.37
			530.4			
PILC-[Ta]5	102.5	74.5	531.8	230.2	0.59	0.36
			530.4			
PILC-[Ta]6	102.4	74.4	531.7	230.2	0.60	0.37
			530.4			
PILC-[Ta]7	102.4	74.4	531.6	230.1	0.69	0.37
			530.4			

DISCUSSION

Texture Evolution and Thermal Stability: Influence of the "mmoles of Tantalum per Gram of Clay" Ratio

XRD and nitrogen adsorption measurements allow the estimation of the effectiveness of the intercalation process. Indeed, the increment observed for the basal spacing and the increase in microporous volume of the Ta-PILCs compared to the initial Na-montmorillonite confirm that the intercalation was successful.

The replacement of Na^+ by tantalum polyhydroxides in the interlayer space results in a large increase in the 2θ value at which the $d(001)$ line of the clay appears. As a result of the intercalation process, the basal spacing of the montmorillonite used in this work (12.4 Å at 120°C) increases to 26–28 Å.

As can be seen in Fig. 1, for a given thermal treatment, Ta-PILCs with a higher tantalum content present sharper and more intense pillared clay diffraction peaks. In fact, for PILC-[Ta]1, PILC-[Ta]2, and PILC-[Ta]3 the pillared clay $d(001)$ diffraction peak is weak and broad, whereas for PILC-[Ta]6, PILC-[Ta]7, and PILC-[Ta]8 the $d(001)$ peak is sharp and intense, indicating a better homogeneity in the spacing between the montmorillonite sheets.

The intercalation of tantalum polyhydroxides between the montmorillonite sheets results in the development of a microporous structure which is maintained even after thermal treatment at 500°C. The introduction of tantalum pillars in the interlayer space keeps the montmorillonite sheets at a certain distance. This system enlargement makes the internal surface area accessible to nitrogen adsorption.

The microporous surface area of the Ta-PILCs, calcined at 500°C, per gram of montmorillonite are displayed in Fig. 11. This standardization has been carried out with the help of the atomic absorption spectrophotometry data.

At 500°C all samples, including those with weak and broad pillar clay $d(001)$ diffraction peaks, present a micropore surface area accessible to nitrogen adsorption. In samples with a low tantalum content, the quantity of pillars is insufficient to maintain the clays sheets apart to a constant distance (32). As a result, the pillared clay $d(001)$ diffraction peak appears weak and broad, a sign of poor homogeneity in the gaps between the sheets. The nitrogen isotherms indicate that even when the space between the clay sheets is not homogeneous, some internal surface area is still accessible.

Regarding thermal stability, all Ta-PILC samples present a similar behavior. After thermal treatment at 500°C, all the Ta-PILCs (PILC-[Ta]4–PILC-[Ta]8) present an interlayer distance of 24–26 Å. The pillar structure (XRD) of Ta-PILCs seems to be maintained up to 600°C (Fig. 1). However, at 700°C, the temperature at which dehydroxylation of the montmorillonite sheets occurs, PILC-[Ta]7 loses its pillared structure (Fig. 3B). Therefore, this thermal instability could be linked to the montmorillonite sheets rather than to the tantalum oxide pillars (33). Indeed, as TGA and DTA thermoanalyses show, the dehydroxylation of the montmorillonite sheets in PILC-[Ta]PILC occurs at a temperature lower than that in Na-montmorillonite. This phenomenon, already observed for aluminum-pillared montmorillonites, has been assigned to dehydroxylation of the pillars. Indeed, with thermal treatment, the pillars dehydroxylate, releasing protons. These protons can migrate through the montmorillonite octahedral sites, inducing pillared structure instability (34, 35).

FIG. 11. Microporous surface area of the Ta-PILCs per gram of montmorillonite.

The XRD diffractograms show that the pillared clay diffraction peak intensity increases with calcination temperature. This phenomenon, unusual in Al-PILCs, has already been observed for Ti-PILCs (36). For titanium-pillared montmorillonites, this intensity increase is a result of the introduction of pillars with different degrees of hydration and hydroxylation into the clay.

After thermal treatment, the dehydrated or dehydroxylated pillars from a well-defined metal oxide size giving rise to uniform spacing of sheets. This assumption is supported by the fact that the basal spacing in tantalum-pillared clays dried at 120°C decreases on an average by about 2 Å when calcined at 500°C.

The atomic adsorption spectrophotometry results show the effective incorporation of tantalum into the clay and confirm the cationic exchange of Na^+ by the tantalum species. The quantity of tantalum incorporated into the montmorillonite initially increases with the tantalum concentration in the intercalation solution. But a saturation plateau is observed at 4.7 mmol of tantalum introduced per gram of clay. This montmorillonite saturation by tantalum polymeric cation is similar to the behavior already described for Ti-PILC (37).

The PILC-[Ta]4, which is the first Ta-PILC to reach the saturation stage, is also the first sample to show a well-resolved pillared clay $d(001)$ diffraction peak.

Nature of the Precursor of the Pillar

On the basis of the bibliographical data concerning tantalum alkoxide hydrolysis and condensation, and taking into account the experimental results obtained for Ta-PILCs ($d(001)$, specific surface area, millimoles of tantalum retained per gram of clay), a structure for the precursor molecule of the tantalum pillars has been proposed.

The first studies carried out on the hydrolysis and condensation of niobium and tantalum alkoxides, which are considered metals having almost identical behaviors, were mainly developed by Bradley (38–40). These works show that in tantalum alkoxide alcoholic solution the tantalum

has an octahedral configuration. The tantalum ethoxide in ethanol is a dimer where the two tantalum octahedra are edge bonded. The hydrolysis of these dimers in water or diluted alcohol results in its condensation, giving rise to $M_{2(x+1)}O_{3x}(OR)_{2(2x+5)}$ type polymeric species. The condensation degree of the oligomers depends on the hydrolysis degree. By increasing the hydrolysis degree ($x=\infty$), insoluble hydrated tantalum oxide polymers are created (41).

However, later studies have shown that the hydrolysis of the transition metal alkoxides can, under certain conditions, via a controlled alkoxolation reaction, lead to the formation of discrete molecules which can be isolated as simple crystals. The existence of these discrete molecules has already been reported for zirconium, titanium, niobium, iron, and chromium (5, 39, 42, 43). For niobium, the only isolated and identified product is $Nb_8O_{10}(OR)_{20}$. Its structure is displayed in Fig. 12. This complex possesses a structure made up of eight octahedra, and is presented as being formed of two M_3O_{13} (three edge-bonded octahedra) groups, which are linked together by two corner-bonded octahedra (44). This molecule has been isolated after a controlled hydrolysis of niobium pentaethoxide in ethanol under conditions very similar to those used for the precursor synthesis of the tantalum pillars (42, 45).

The complex obtained in this way has a rather spherical shape. The dimension of this complex estimated from the structural data published by Bradley is 14.5–16.5 Å. The estimated basal spacing that would result with the introduction of this complex between the montmorillonite sheets, 14.5–16.5 Å plus 9.6 Å for the montmorillonite sheet thickness, fits well with the values obtained for Ta-PILCs.

The validity of the proposed molecule as a pillar of the Ta-PILC structure has been confirmed by comparing the micropore surface area developed by these solids with the theoretical micropore surface area that the $[Ta_8O_{10}(OR)_{20}]$ homogeneous arrangement in the interlayer space would generate. According to the atomic absorption spectrophotometry results, a gram of montmorillonite fixes a maximum of about 4.5 mmol of $[Ta]_8$ complex. To calculate the theoretical surface, the $[Ta_8O_7(OR)_{20}]$ complex has been considered a sphere of 15.0 Å diameter.

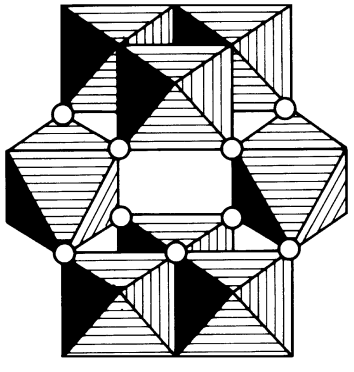

FIG. 12. Proposed structure for $[Nb_8O_{10}(OR)_{20}]$.

The interlayer space blocked by the pillars will be (46)

$$S_{[Ta]_8} = \left(\frac{4.5\times10^{-3}}{8}\right)\cdot N_A\cdot\pi\cdot\left(\frac{15\times10^{-10}}{2}\right)^2 = 598\,m^2/g.$$

If the theoretical surface area developed by Na-montmorillonite is 700 m^2/g, the theoretical interlayer surface area remaining accessible would be

$$S_{(Ta\text{-}PILC)theor.} = S_{Na^+\text{-}mont.} - S_{[Ta]_8} = 700 - 598$$
$$= 102\,m^2/g \text{ of clay.}$$

The theoretical value obtained is of the same order as the microporous surface area calculated by nitrogen adsorption.

The micropore size distribution curves show the existence of pores of 6.6 Å diameter within the Ta-PILC. Therefore, there is a disagreement between the XRD analysis showing a 15-Å separation between the montmorillonite sheets, and the pore diameters calculated from the micropore size distribution, 6.6 Å.

To understand the validity of these two techniques it is necessary to note that, in pillared clays, the micropores are characterized by two different dimensions (47): first, the size of the pillars, and second, the distance between them. Supposing a homogeneous arrangement of the pillars in the interlayer space, the distance between pillars can be calculated as

$$D = \sqrt{\frac{102\times10^{+20}}{\frac{4.5\times10^{-3}}{8}\cdot N_A}} = 5.5\text{ Å}.$$

Taking into account that neither the exact quantity of tantalum introduced into the interlayer space nor the precise size of the pillars is known, this simple estimate provides a good approximation and shows that the maximum measured by the micropore size distribution curves (6.6 Å) can be assigned to the distance between the tantalum oxide pillars.

The last calculations show a high density of pillars in the interlayer space. This phenomenon can be understood supposing a quite low charge average of pillars. Accordingly, the cationic exchange will lead to a dense arrangement of pillars.

Interaction between Tantalum Oxide and Montmorillonite

Under the intercalation conditions, small particles of amorphous tantalum oxide have been synthesized. In fact, transmission electron microscopy does not show isolated tantalum oxide particles. This indicates that the tantalum is incorporated in the clay matrix without forming aggregates (50 nm).

The dispersion of amorphous tantalum oxide within the montmorillonite is confirmed by DTA curves. The temperature at which the tantalum oxide crystallizes in the pillared clays is 870°C. Under the same thermal treatment, the nondispersed tantalum oxide crystallizes at 760°C. These curves show that, as a result of the amorphous tantalum oxide dispersion, the temperature at which the tantalum oxide crystallizes in Ta-PILCs is delayed by 100°C. These observations agree with the X-ray diffractograms carried out after thermal treatment of Ta-PILCs at 700 and 900°C. A similar crystallization delay has already been observed for Zr-PILC (32, 48).

The Ta-PILCs with lower tantalum contents (samples PILC-[Ta]1, PILC-[Ta]2, and PILC-[Ta]3) do not present, for the temperature interval studied (up to 1000°C), any tantalum oxide crystallization exothermic peak. In samples with a lower tantalum content, the dispersion of tantalum oxide within the montmorillonite layers prevents tantalum oxide crystallization. The amorphous structure of tantalum oxide could be stabilized by the interaction with the montmorillonite layer.

As described above, a homogeneous spacing between the montmorillonite layers is obtained for tantalum contents higher than those used for PILC-[Ta]4. However, as shown by XRD and TGA, this high tantalum content leads to easier sintering and crystallization of tantalum oxide.

In the region 500–900 cm^{-1} of the FTIR spectra, the superposition of the clay structure vibration modes with the broad band of the Ta–O vibration modes makes its interpretation difficult. However, these FTIR spectra clearly show that the characteristic bands of the Ta–O stretching modes are mainly observed from the PILC-[Ta]4 sample.

The presence of pillars in the interlayer space is confirmed by the shift of the vibration band assigned to the OH groups in the $(Al, Mg–OH)_{octahedra}$ bond. Indeed, compared with Na-montmorillonite, the vibration frequency of this band shifts to a higher value (cm^{-1}) when the tantalum oxide is incorporated within the clay. The shift of this vibration band corresponding to the OH groups of the clay octahedral sheets has already been correlated in the literature with the nature of cations located in the interlayer space. Different phenomena can bring about this band shift: (i) The hexagonal holes on the montmorillonite layers are currently admitted as the place for the direct interaction between the intercalated cation and the oxygen on the clay surface. These holes allow the cation to approach the negative potential located in the octahedral sheets and, from them, to interact with octahedral OH groups (49). (ii) The (H^+) cation migration toward the octahedral positions after thermal treatment can also be at the origin of this shift due to the change in the hydroxyl group orientation (50). (iii) Thomas and co-workers (51), suggested that in PILCs the condensation of the OH terminal groups of the polymeric ions (pillars) with the OH groups of the clay octahedral sheets can form a bond, which can also explain the shift of the vibration band toward higher (cm^{-1}) values.

However, the existence of mechanisms (ii) and (iii) in Ta-PILCs would involve a sharp decrease in the intensity of this band (50, 51), and such a decrease is not observed in the FTIR spectra.

As shown by XPS analysis, the tantalum binding energy in Ta-PILC corresponds to that of pure tantalum oxide (31). This result indicates that, on average, the intercalated cation is not greatly influenced by the negative charge of the montmorillonite layer. In the same way, the binding energies of the montmorillonite constitutive elements are maintained after intercalation. However, as bulk Ta/Al and Ta/Si ratios, obtained by atomic absorption spectrophotometry, are systematically larger than those obtained by XPS surface analysis, it can be deduced that the tantalum is mainly distributed in the montmorillonite interlayer space (52).

Origin of the Macromesopores

The adsorption–desorption isotherms show that the tantalum-pillared montmorillonite possesses, in addition to the microporous structure, a meso- and a macroporous structure. Moreover, the existence of a macromesoporous structure was already observed in the initial nonpillared Na-montmorillonite.

As the microporosity within the pillared clays is the result of the intercalation of the pillars between the clay layers, the macromesoporosity observed within the Ta-PILC can be considered a result of the drying method used for its synthesis.

Figure 13 displays the adsorption–desorption isotherms for one Ta-PILC (PILC-[Ta]6 preparation) dried in its oriented and nonoriented form. For the oriented sample, a concentrated suspension of pillared clay has been deposited onto large glass slides. The suspension has been allowed to dry at room temperature for 2 days and finally dried at 120°C. This method favored the sediment of the clay layers oriented horizontally. For the nonoriented sample, the pillared clay was dried at room temperature without bringing out any preferential orientation, namely as all the samples of the above-studied series.

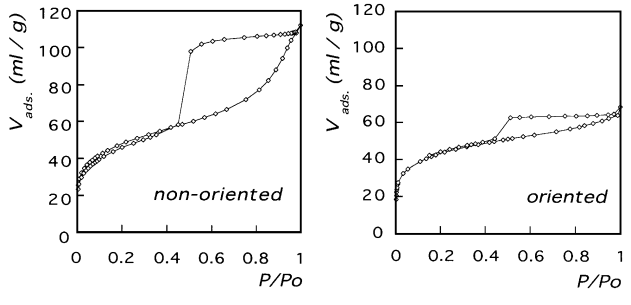

FIG. 13. Nitrogen adsorption–desorption isotherms for a Ta-PILC (PILC-[Ta]6) dried in its oriented and nonoriented forms.

As can be seen in Fig. 13, the method used for drying the Ta-PILCs influences the external surface area developed by the clays. The external surface area is much less marked in oriented pillared clays than in nonoriented ones. For oriented samples, a type I adsorption isotherm with an H4 hysteresis loop, characteristic of pillared clay microporous structure, is found.

It is interesting to note that the microporosities developed for the two samples are almost identical. In fact, the α_S-plot curves show that the microporous surface area (approximately 110 m^2/g) is almost identical for both of them, whereas the external surface area ranges from 65 to 19 m^2/g for the nonoriented and the oriented samples, respectively.

The microporosity in PILCs is essentially correlated with interlayer galleries. The association of layers of pillared clays leads to the formation of elementary particles: tactoïdes. Within the tactoïdes, the mesoporosity can be produced by the holes generated between the layer breaks. The irregular pile of tactoïdes can bring about some macro- and mesoporosity. Among the mesoporous, these angle-shaped particles cannot produce a hysteresis loop since in this type of pores the adsorption–desorption process is identical (53).

The method chosen for drying influences the arrangement of the aggregates of the pillared clays. Oriented drying reduces the free spaces between aggregates. Nonoriented drying increases the layers disorder and the meso-macropores present in the solid are more numerous. The pillared clay microporous structure is formed during the clay suspension intercalation and it is not essentially altered by the choice of the drying method.

Influence of the Atomic Weight of Tantalum upon the Ta-PILC Specific Surface Areas

The specific surface areas developed by the tantalum-pillared clays are appreciably lower than the characteristic surface areas (m^2/g) of the most often studied pillared clays: Al-, Zr-, and Ti-PILC (54). This can, in part, be explained by the high atomic weight of the tantalum. Indeed, whereas aluminum, titanium, and zirconium possess atomic weights in the range between 27 and 91.2 g, the atomic weight of tantalum is 181 g.

As a result, the intercalation of 4 mmol of metal per gram of clay represents 0.16 and 0.08 g of titanium and aluminum per gram of Ti- and AL-PILC, respectively. However, for Ta-PILC, this ratio is 0.42 g of tantalum per gram of Ta-PILC. This means that for the same pillar density a gram of tantalum-pillared montmorillonite contains much less clay than a gram of aluminum- or titanium-pillared montmorillonite. From then on, the micropore surface area and the micropore volume per gram of pillared clay will be systematically lower for Ta-PILC than for its homologous Ti- or Al-PILC.

CONCLUSIONS

The controlled hydrolysis of the tantalum ethoxide $Ta(OC_2H_5)_5$ in alcoholic solution has allowed us to set up an effective method for the synthesis of a new family of pillared clays: Ta-PILCs.

The initial advantage of this method, compared with the synthesis of Ta-PILCs from tantalum clusters $(Ta_6Cl_{12})^{2+}$ described by Christiano *et al.*, is its simplicity. Indeed, this new intercalation method does not require preliminary synthesis of the pillar precursor. This will greatly simplify catalyst synthesis.

In addition, contrary to the pillared clays synthesized from tantalum clusters, this new Ta-PILC family presents very interesting physicochemical properties, namely a high thermal stability (the pillared structure is preserved even after calcination at 600°C) and the basal spacing, 26 Å at 500°C, is one of the greater values described in the literature.

The effective incorporation of tantalum within the clay, by the cationic exchange of Na^+ by tantalum species, is confirmed by the atomic absorption spectrophotometry measurements carried out upon the pillared clays.

Moreover, the development within the Ta-PILC of a microporous structure, characteristic of pillared clays, has been confirmed by textural analysis (nitrogen adsorption/desorption isotherms, α_S-plot curves, and nitrogen adsorption isotherms at very low pressures). Additional evidence of the effective incorporation of the tantalum is: (i) the microanalyses carried out by TEM, where tantalum oxide aggregates cannot be detected, and (ii) the delay in the Ta_2O_5 crystallization process observed by XRD and DTA in Ta-PILCs compared to pure tantalum oxide.

The quantity of tantalum used in the intercalation process seems to have very important repercussions upon the texture of the resulting Ta-PILC. A minimal quantity of tantalum is necessary for obtaining Ta-PILCs characterized by a sharp and intense pillared clay $d(001)$ peak, a sign of good homogeneity in the gap between the montmorillonite sheets. The accessibility to the internal structure of the Ta-PILC seems to increase with the initial quantity of tantalum.

On the basis of bibliographical data concerning hydrolysis and condensation of tantalum alkoxides, and taking into account the experimental results obtained for this series of Ta-PILCs, a structure type $[Ta_8O_{10}(OR)_{20}]$, $R = H$, C_2H_5, has been proposed as the precursor molecule of the tantalum pillars.

ACKNOWLEDGMENTS

We thank "Eusko Jaurlaritza" (Grant BFI90.061 modalidad AK) and the Service de la Programmation de la Politique Scientifique, Belgium, for financial support. We express our thanks to Dr. T. Curtin for reviewing the manuscript.

REFERENCES

1. Thomas, J. M., and Theocharis, C. R., *in* "Perspectives in Catalysis" (J. M. Thomas and K. I. Zamaraev, Eds.), p. 465. Blackwell Scientific, Oxford, 1992.
2. Figueras, F., *Catal. Rev. Sci. Eng.* **30**, 457 (1988).
3. Tanabe, K., "Solid Acids and Bases: Their Catalytic Properties." Academic Press, New York/London, 1970.
4. Tanabe, K., Misono, M., Ono, Y., and Hattori, H., *in* "New Solid Acids and Bases: Their Catalytic Properties" (B. Delmon and J. T. Yates, Eds.), Studies in Surface Science and Catalysis, Vol. 51. Elsevier, New York, 1989.
5. Ushikubo, T., and Wada, K., *Appl. Catal.* **67**, 25 (1990).
6. Ushikubo, T., and Wada, K., *J. Catal.* **148**, 138 (1994).
7. Livage, J., Henry, M., and Sanchez, C., *Prog. Solid State Chem.* **18**, 259 (1988).
8. Lassner, E., and Püschel, R., *in* "Chelates in Analytical Chemistry" (H. A. Flaschka and A. J. Barnard, Eds.), Vol. 2, p. 213. 1969.
9. Christiano, S. P., Wang, J., and Pinnavaia, T. J., *Inorg. Chem.* **24**, 1222 (1985).
10. Harned, H. S., Pauling, C., and Corey, R. B., *J. Am. Chem. Soc.* **82**, 4815 (1960).
11. Guiu, G., and Grange, P., *J. Chem. Soc., Chem. Commun.*, 1729 (1994).
12. Farfan-Torres, E. M., Sham, E., and Grange, P., *Catal. Today* **15**, 515 (1992).
13. Bhambhani, M. R., Cutting, P. A., Sing, K. S. W., and Turk, D. H., *J. Colloid Interface Sci.* **38**, 109 (1972).
14. Jaroniec, M., Choma, J., Swiatkowski, A., and Radeke, K. H., *Chem. Eng. Sci.*, 3151 (1988).
15. Defossé, C., *in* "X-Ray Photoelectron Spectroscopy" (F. Delannay, Ed.), Characterization of Heterogeneous Catalysts, p. 225. Dekker, New York, 1984.
16. Balachandran, U., and Eror, N. G., *J. Mater. Sci. Lett.* **1**, 219 (1982).
17. Vieira Coelho, A., and Poncelet, G., *Appl. Catal.* **77**, 303 (1991).
18. Yamanaka, S., and Brindley, G. W., *Clays Clay Miner.* **27**, 119 (1979).
19. Occelli, M. L., Landau, S. D., and Pinnavaia, T. J., *J. Catal.* **104**, 331 (1987).
20. Horvath, G., and Kawazoe, K., *J. Chem. Eng. Jpn.* **16**, 470 (1983).
21. Gil, A., and Montes, M., *Langmuir* **10**, 291 (1994).
22. Van der Marel, H. W., and Beutelspacher, H., "Atlas of Infrared Spectroscopy of Clay Minerals and Their Mixtures." Elsevier, Amsterdam, 1976.
23. Farmer, V. C., *in* "Data Handbook for Clay Materials and Other Nonmetallic Minerals" (H. Van Olphen and J. J. Fripiat, Eds.), p. 285. Pergamon Press, Elmsford, NY, 1979.
24. Shimoda, S., and Brydon, J. E., *Clays Clay Miner.* **19**, 61 (1971).
25. Djordjevic, C., and Katovic, V., *J. Less-Common Metals* **24**, 325 (1970).
26. Phulé, P. P., *J. Mater. Res.* **8**, 334 (1993).
27. Yamaguchi, O., Tomihisa, D., Uegaki, T., and Shimizu, K., *J. Am. Ceram. Soc.* **70**, 335 (1987).
28. Légaré, P., and Fritsch, A., *Surf. Interface Anal.* **15**, 698 (1990).
29. Remy, M. J., Genet, M. J., Poncelet, G., Lardinois, P. F., and Notté, P. P., *J. Phys. Chem.* **96**, 2615 (1992).
30. Seyama, H., and Soma, M., *J. Chem. Soc., Faraday Trans.* **80**, 237 (1984).
31. Guiu, G., and Grange, P., *Bull. Chem. Soc. Jpn.* **67**, 2716 (1994).
32. Farfan-Torres, E. M., Dedeycker, O., and Grange, P., *in* "Preparation of Catalysts V" (G. Poncelet, P. A. Jacobs, P. Grange, and B. Delmon, Eds.), Studies of Surface Science and Catalysis, p. 337. Elsevier, Amsterdam, 1991.
33. Auer, H., and Hofmann, H., *Appl. Catal.* **97**, 23 (1993).
34. Tichit, D., Mountassir, Z., Figueras, F., and Auroux, A., *in* "Preparation of Heterogeneous Catalysts" (G. Poncelet, P. A. Jacobs, P. Grange, and B. Delmon, Eds.), Studies of Surface Science and Catalysis, Vol. 63, p. 345. Elsevier, Amsterdam, 1990.
35. Tichit, D., Faula, F., Figueras, F., Ducorant, B., Mascherpa, G., Gueguen, C., and Bousquet, J., *Clays Clay Miner.* **36**, 369 (1988).
36. Del Castillo, H. L., Gil, A., and Grange, P., *J. Phys. Chem. Solids*, in press.
37. Sterte, J., *Clays Clay Miner.* **34**, 658 (1986).
38. Bradley, D. C., *in* "Advances in Inorganic Chemistry and Radiochemistry. Metal Alkoxides and Dialkylamines" (H. J. Emeleus, Ed.), p. 259. Academic Press, London, 1972.
39. Bradley, D. C., and Holloway, H., *Can. J. Chem.* **39**, 1818 (1961).
40. Bradley, D. C., and Holloway, H., *Can. J. Chem.* **40**, 62 (1962).
41. Merhotra, R. C., *J. Non-Cryst. Solids* **100**, 1 (1988).
42. Kepert, D. L., "The Early Transition Metals," Chap. 3, p. 142. Academic Press, London, 1972.
43. Drljaca, A., Anderson, J. R., Spiccia, L., and Turney, T. W., *Inorg. Chem.* **31**, 4894 (1992).
44. Bradley, D. C., Hurthouse, M. B., and Rodesiler, P. F., *J. Chem. Soc., Chem. Commun.*, 1112 (1968).
45. Bradley, D. C., *Coord. Chem. Rev.* **2**, 299 (1967).
46. Chevalier, S., Franck, R., Lambert, J. F., Barthomeuf, D., and Suquet, H., *Appl. Catal.* **110**, 153 (1994).
47. Gil, A., Massinon, A., and Grange, P., *Microporous Mater.* **4**, 369 (1995).
48. Occelli, M. L., *J. Mol. Catal.* **35**, 37 (1986).
49. Miller, S. E., Heath, G. R., and Gonzalez, R. D., *Clays Clay Miner.* **30**, 11 (1982).
50. Calvet, R., and Prost, R., *Clays Clay Miner.* **19**, 175 (1971).
51. Tennakoon, D. T. B., Jones, W., and Thomas, J. M., *J. Chem. Soc. Faraday Trans. I* **82**, 3081 (1986).
52. Martin-Luengo, M. A., Martins-Carvalho, H., Ladriere, J., and Grange, P., *Clay Miner.* **24**, 495 (1989).
53. Gregg, S. J., and Sing, K. S. W., "Adsorption, Surface Area, and Porosity," Academic Press, London, 1982.
54. Del Castillo, H. L., Gil, A., and Grange, P., *Catal. Lett.* **43**, 133 (1997).